

We are IntechOpen, the world's leading publisher of Open Access books Built by scientists, for scientists

6,100

Open access books available

167,000

International authors and editors

185M

Downloads

Our authors are among the

154

Countries delivered to

TOP 1%

most cited scientists

12.2%

Contributors from top 500 universities



WEB OF SCIENCE™

Selection of our books indexed in the Book Citation Index
in Web of Science™ Core Collection (BKCI)

Interested in publishing with us?
Contact book.department@intechopen.com

Numbers displayed above are based on latest data collected.
For more information visit www.intechopen.com



Failure Analysis of Steam Generator Tubes

Gonzalo Diego and Susana Merino

Abstract

Steam generator fabricated of alloy 600 tubes has been replaced in the last decades by newer versions built with alloy 690 or alloy 800 tubes. At first, it was thought that both alloys were resistant to SCC mechanisms but after several years of operation, some NPPs developed denting processes and IGSCC, especially in alloy 800. Corrosion products accumulated in the crevice area between tube-sheet and secondary tube surface of SG increase the stresses and produce a chemical more aggressive to the environment. These two points are the main factor to occur “denting” and increase the possibility of ODSCC can be developed. This chapter describes the failure analysis of an alloy 800 SG tube with only nine years of operation. Microstructural characterization of sludge was carried out after the cleaning by mechanical tube sheet water lancing. SEM/EDX, surface analysis by Auger, and XPS spectroscopy were used to identify chemical species over the OD surface and the fracture surface of some open cracks. “Denting” mechanism is related to flow accelerated corrosion and oxidant particles introduced into secondary side of SG. Therefore, it is convenient to prevent the impurities intake into SG and perform a chemical cleaning process to avoid the hard sludge formation.

Keywords: steam generator (SG), denting, intergranular stress corrosion cracking (IGSCC), alloy 800

1. Introduction

Nuclear power plants steam generators (NPPs SGs) are normally vertical cylindrical vessels made up of inverted U-tubes and with steam-water separators at the top of the device. Boiling occurs on the shell side named the secondary side while on the primary side, inside of the tubes, the coolant never reaches the state of steam (310–330°C and 15 MPa). Most NPPs PWR have between two and four SGs.

Actually, most steam generator tubes are fabricated with thermally treated Alloy 690 even though is still supplied with replacement Alloy 800NG tubing. In this manner, progressively replacing Alloy 600 MA has been performed due to many failures caused by stress corrosion cracking (SCC) in this alloy. **Figure 1** shows a Fe-Cr-Ni ternary diagram where is shown the composition of the alloys used in nuclear power plants.

Alloy 690 is a solid substitutional alloy consisting of approximately 60% nickel, 30% chromium, and 10% iron. The concentration limits of these elements as well as

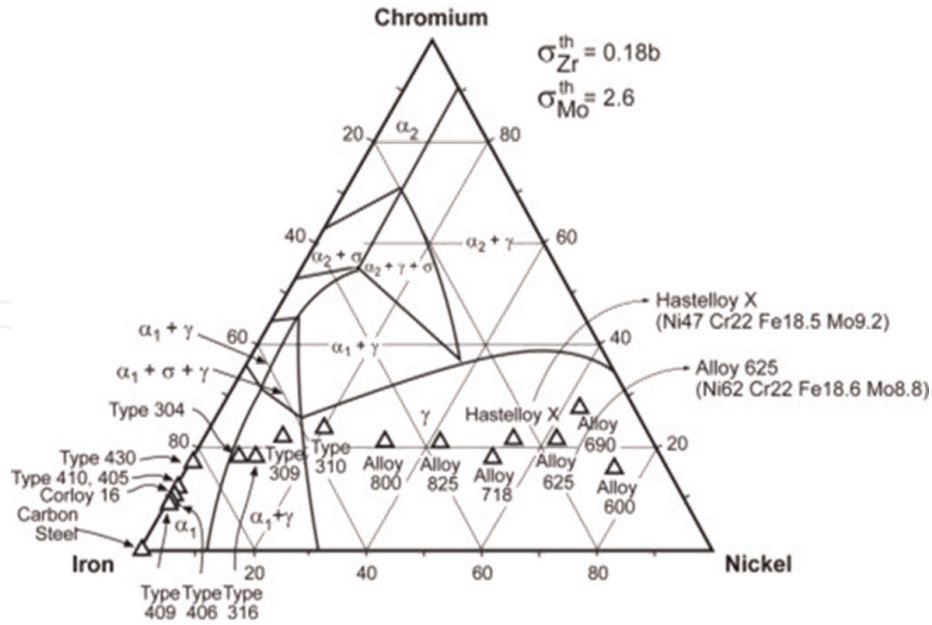


Figure 1.
Fe-Cr-Ni ternary diagram for 400°C for NPPs SGs [1].

Standard	Designation
ASTM/ASME	B163/SB163
UNS	N06690
DIN	17,459
ISO	NiCr29Fe9
AFNOR	NC30Fe

Table 1.
Designations for alloy 690.

the rest of the constituent elements present slight differences depending on the manufacturer or institution that sets the specification. **Table 1** presents various designations and standards for this alloy. The chemical composition of alloy 690 is listed in **Table 2**.

The control of carbon within the limits established according to **Table 2** is essential to obtain the desired corrosion resistance and mechanical properties. In general, a maximum limit is established, although in some specifications a minimum limit is indicated [2]. Carbon range between 0.015 and 0.025% is the optimum to obtain a microstructure with inter and intragranular carbide precipitation. The lower carbon limit (0.015%) is necessary to ensure enough carbon is available for correct carbide precipitation. The upper limit (0.025%) is specified to ensure that most of the carbides formed can be dissolved during mill-annealing heat treatment [3]. Limits have also been specified for sulfur and phosphorus since these elements could segregate at grain boundaries and have a detrimental effect on corrosion resistance. In addition, sulfur decreases the ability of these alloys to be hot worked, so it is necessary to keep its level at low values.

On the other hand, Alloy 800 is an alloy closer to titanium stabilized stainless steel. This alloy has been used for industrial applications with slight differences in its composition and with different thermal treatments to ensure optimal behavior in the

Chemical Requirements (ALLOY 690)	
Nickel	remainder
Chromium	27.0–31.0
Iron	7.0–11.0
Manganese	0.50 max.
Carbon	0.05 max.
Copper	0.50 max
Silicon	0.50 max
Sulfur	0.015 max.

Table 2.

Composition limits, %. ASTM designation B163 or ASME SB163: “Standard Specification for Seamless Nickel and Nickel Alloy Condenser and Heat-Exchanger Tubes.”

operating environment. In the nuclear industry, the composition and heat treatment of alloy 800 has been optimized, establishing a clear difference between the standard alloy and its modified version named modified alloy 800, **Table 3**.

The compositional variations introduced in the alloy 800 have important repercussions in terms of the corrosion resistance of this material (**Table 4**). For example, the reduction of the carbon content to 0.03% and the stabilization ratio $Ti/C > 12$ and $Ti/C + N > 8$ have been established to ensure good resistance to sensitization and, therefore, resistance to intergranular corrosion in conditions representative of acid-sulfate chemistry. In addition, the total amount of aluminum and titanium is important. $Al + Ti$ contents above 0.55%, produce the precipitation of γ' phase ($Ni_3(Al, Ti)$) when the material is subjected to thermal treatments between 500 and 700°C. This gamma phase and the $M_{23}C_6$ type carbides produce an increase in creep resistance with a clear decrease in ductility [4, 5]. Increasing the minimum chromium level to 20% results in good pitting corrosion resistance. On the other hand, increasing the minimum nickel content to 32% is intended to improve resistance to transgranular stress corrosion cracking.

Most of the failures that occur in NPPs SGs tubes involve various mechanisms, including:

- High cycle of fatigue in the tube support plate (TSP)
- Primary water stress corrosion cracking (PWSCC)
- Outer diameter stress corrosion cracking (ODSCC)

Standard	Designation
ASTM/ASME	B163/SB163
UNS	N08800
EN	2.4642 - NiCr29Fe
ISO	6207
AFNOR	Z5 NC 35–20

Table 3.

Designations for alloy 800.

Chemical Requirements (alloy 800)	
Iron	remainder
Niquel	30.0–35.0
Chromium	19.0–23.0
Manganese	1.50 max.
Carbon	0.10 max.
Copper	0.75 max
Silicon	1.0 max
Sulfur	0.015 max.
Aluminum	0.15–0.60
Titanium	0.15–0.60

Table 4. Composition limits, %. ASTM designation B163 or ASME SB163: “Standard Specification for Seamless Nickel and Nickel Alloy Condenser and Heat-Exchanger Tubes.”

- Tube support denting (TSD)
- Fretting
- Others: pitting, wastage.

Most nuclear power plants operate under AVT (all-volatile treatment) conditions on the secondary side of the steam generators. Common volatile conditioning agents are ammonia, amines, and hydrazine (or hydrazine substitutes). With AVT, the pH of the feed water ranges from 8.8 to 9.8.

During normal operation of the SGs, nonvolatile compounds rise to a concentration level higher than the feed water. For this reason, the SGs are periodically purged using continuous blowdown. Although this operation should be sufficient to avoid corrosion damage, the permanent ingress of corrosion products produces deposits accumulation on the tube-sheet increasing the risk of the initiation corrosion process. Physical and chemical changes may occur depending on the impurities level in the deposits or the sludge composition, such as solubility product, precipitation of compounds, hydrolysis, etc [6]. Impurity sources can be treatment plant quality, cooling water (condenser leaks), repairs and impurities in conditioning chemicals, etc. The insulating effect of a deposit of corrosion products can cause overheating of the tube metal and subsequent failure. Because they are generally porous, corrosion product deposits can also provide sites for boiler water concentration and thus the potential for caustic attack. In general, the concentration of species due to the presence of crevices and sludge accumulation gives rise to acidic or basic environments far away from normal secondary chemical conditions.

For this reason, many nuclear plants periodically perform sludge removal by tube-sheet lancing (SL) and inner bundle lancing (IBL) on the steam generator's secondary side. Lancing uses high-pressure jets to mechanically remove sludge from the tube-sheet surface, and in this way, impurities concentration is eliminated and denting formation is avoided.

2. Experimental procedure

The failure analysis was performed on the steam generator tube in different areas with circumferential cracks previously detected using Eddy current and UT technique. Three areas were characterized on the surface of the tube, called: the free tube, transition zone, and expanded zone (**Figure 2**). Using the stereo microscope, the area of interest was identified and isolated by a silicon carbide disc cutter. The cutting procedure was dry, without refrigeration, so as not to disturb the composition of the existing deposits on the external surface.

The characterization of the deposits was performed by EDX, XPS, and XRD. These deposits or sludge frequently accumulate in the area of the tube sheet.

The characterization of the fracture surface was performed by longitudinally cutting the tube into two equal half parts. One of them was tested for fatigue to obtain the fracture surfaces (**Figure 3**).

The fracture surface was examined on SEM to quantify the length and depth of existing cracks. The deposits found on the fracture surface of the two cracks were analyzed by EDX and by Auger spectroscopy, five zones of each crack from OD, (point 1) to inside the crack (point 5) (**Figure 4a**).

Metallographic characterization of the axial sections was carried out on the other half of the tube piece as shown in **Figure 4b**.

In addition, the microstructural characterization of the hard sludge steam generator has been carried out. The samples to be examined were collected during the last cycles and appeared in form of deposits or sludge and accumulate in the area of the tube sheet. All samples were weighed and dried at 60° for 48 hours and then classified by sieve size into three types: dust (D), small size (SS), and large size (LS). Microstructural and physical characterization of each individual particle was also performed using SEM and EDX analysis, stereomicroscope, and microhardness.

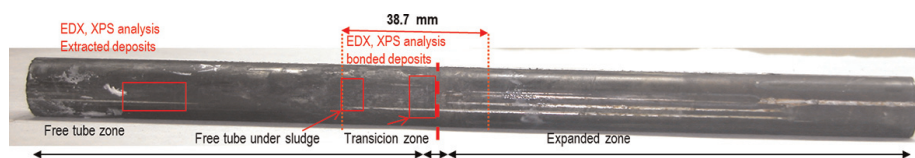


Figure 2.
As-reception segment tube. showing deposits analysis areas.

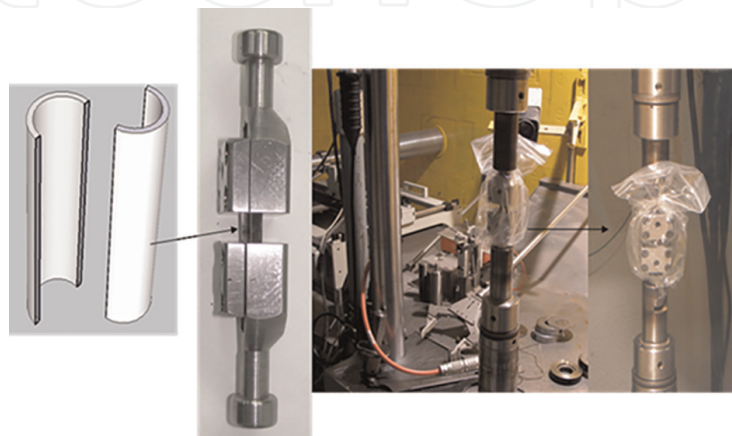


Figure 3.
Devices used to obtain the fracture surface.

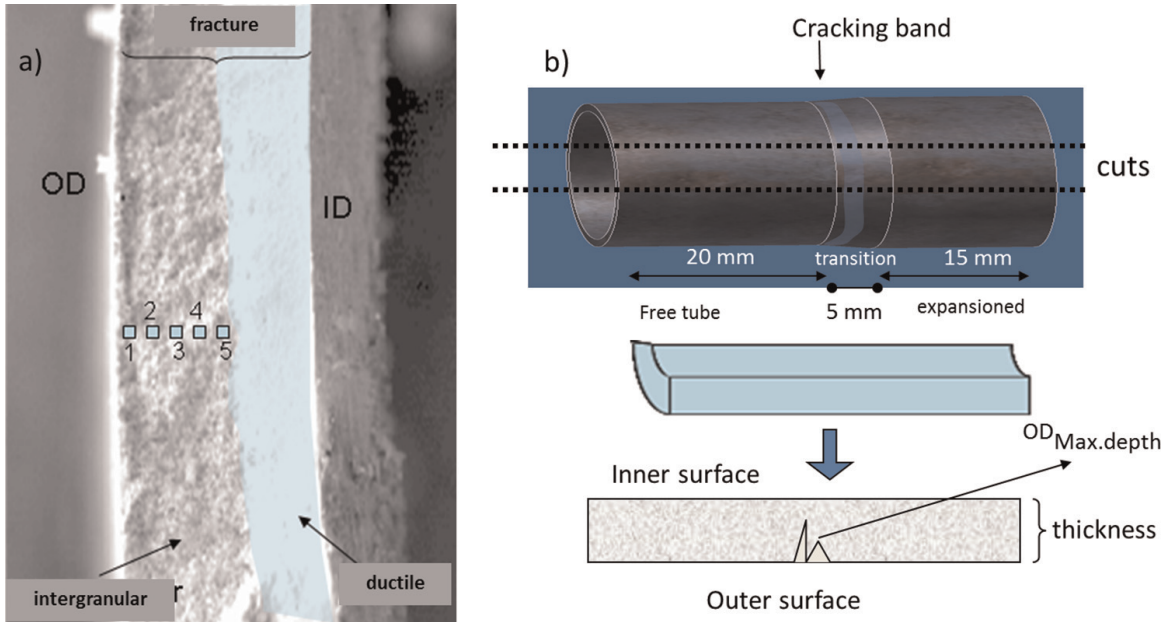


Figure 4. a) Points analyzed on the fracture surface by Auger spectroscopy. b) Metallographic specimens from the other half of the tube in the area of interest.

3. Results

3.1 Visual inspection

Circumferential cracks and denting were detected by Eddy's current technique before the extraction in the expanded transition zone. Three different areas were identified for subsequent tests: free tube, transition zone, and expanded zone (Figure 5a). Zero is also marked for recording observations collected along the tube perimeter.

Multiple circumferential small cracks separated by ductile ligaments in an area of 5 mm width are shown in Figure 5b. These cracks were located at 3 mm from the last contact point between the tube and the tube sheet. Damage as "wastage," pitting or other has not been detected. Different color is observed among these areas. The expanded region shows a red coloration (tube sheet contact) while the transition zone presents a dark gray color because this area has been covered by sludge.

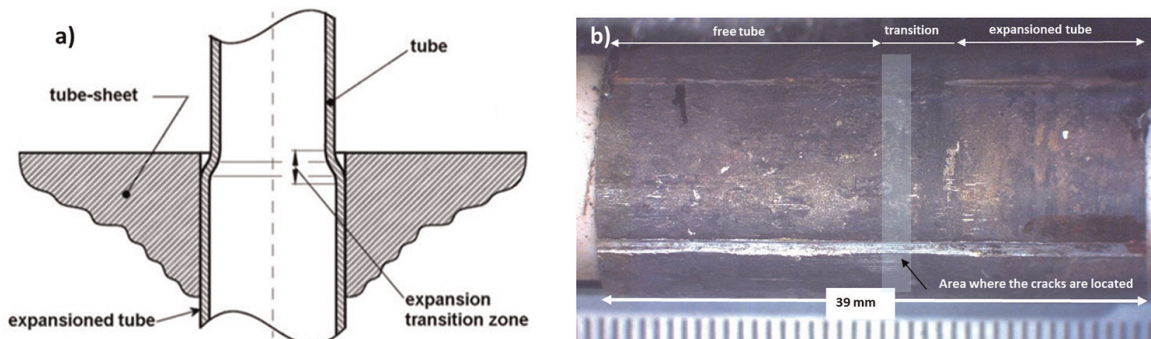


Figure 5. a) As-reception segment tube extracted in the area of the sketch. b) Image analysis to detect the expansion end of the tube by stereoscopy microscopy.

3.2 Deposits characterization on free tube under sludge.

Table 5 shows a comparative analysis of the deposits removed from the free tube surface. EDX results of sludge deposits, located in the expansion transition and extracted in the free tube, indicate a process of impurities concentration on the crevice area formed between the tube sheet and the tube. Significant concentrations of Si, Mg, Ca, S, Cu, Zn, Na, and Cl were detected. This process of impurity concentration is not as evident in the top of the sludge area where EDX analysis indicates that the detected impurities are present only in part of the analyses. Moreover, Pb has been found in low concentrations.

XPS and XRD results of these deposits showed the existence of metallic Cu and FeS₂, which correspond to reducing environment of the typical operation secondary side in SG. Likewise, reduced sulfur species, such as sulfides or sulfites, were detected in the expansion transition zone and the area under sludge. Moreover, XPS has identified the presence of metallic Fe and Cr in the free tube under the sludge.

Other compounds identified are a mixture of silicates, mainly of Al, and Mg. Na is sometimes associated with Cl and S, although this association is qualitative by EDX analysis. XPS analysis has identified the presence of Ca (as Ca chlorides) and a mixture of metallic oxides with K and Mg. S is detected in both oxidized and reduced forms, like sulfates and sulfides.

A comparative XPS analysis of deposits at both free tube and expansion transition zone is summarized in **Table 6**. Fe is detected as magnetite and mixed spinels. Metallic Fe is present in the free tube deposits of the surface and is not detected in the transition area. Al-silicates with Mg, Na, CaCl₂, and S, like sulfates and sometimes as sulfites, are detected in both areas.

3.3 Cracking characterization on OD side

Figure 6a) shows the cracks detected on the OD side of the tube. Cracks have a circumferential orientation with corrosion deposits and they were detected in an area around the tube located above the last point of contact between the tube and tube sheet. The highest density of the cracks was located at 5 mm of this last point.

Figure 6b) shows the intergranular morphology of the cracks at high magnification and the aspect of the corrosion deposits on the tube surface. EDX analyses show important amounts of Na, Si, S, and Cl in these areas. Also, the presence of Cu and traces of Pb and Zn were also detected in five analyses.

Elements	EDX	XPS	DRX
Fe	M: 41% atomic	M: Magnetite and spinels. Hidróxide and Fe metallic.	M: Spinels and sulfide form
Mg, Al y Si	M: 29% atomic	M: Al Silicates	—
Na, K, Mg, Ca	M: 25% atomic (all elements)	X: CaCl ₂ , only detected	X: Ca, K y Mg as mixed metallic oxides.
Cr, Ni*, Mn, Ti	X: Cr*, Ni*	X: Spinels, mixed oxides	X: Spinels, mixed oxides
Cu, Zn	X	X: Cu met. and óxide Cu+.	X: Cu+, as (KCuO ₂)
P, S y Cl	X	X: Cl-	X: Sulfides and sulfates

*Possibility of these elements belongs to base material. M: Majority phase or element; X: Minority phase or element.

Table 5.
 Overview of EDX, XPS and XRD analyses on deposits removed from the free surface of the tube.

Element	Free tube under sludge	Transition zone
Fe	Fe ₂ O ₃ / Fe ₃ O ₄ , FeO, metallic Fe	Fe ₃ O ₄ , FeO, FeSO ₄
Ni	NiO (probably)	**
Cr	Cr ₂ O ₃ , spinels of Fe, Cr	**
Ca	CaCl ₂	CaCl ₂ , silicates
Cl	chlorides	chlorides
S	sulfides *	Sulfates, sulfites
Si	Silicates, SiO ₂	Silicates, SiO ₂
Al	Al ₂ O ₃ , Al(OH) ₃ , silicates	Al ₂ O ₃ , silicates
Mg	Silicates, oxide	Silicates, oxide

* sometimes as sulfites
 ** minority phase (mixed oxides)

Table 6.
 XPS analysis on free tube under sludge and transition area.

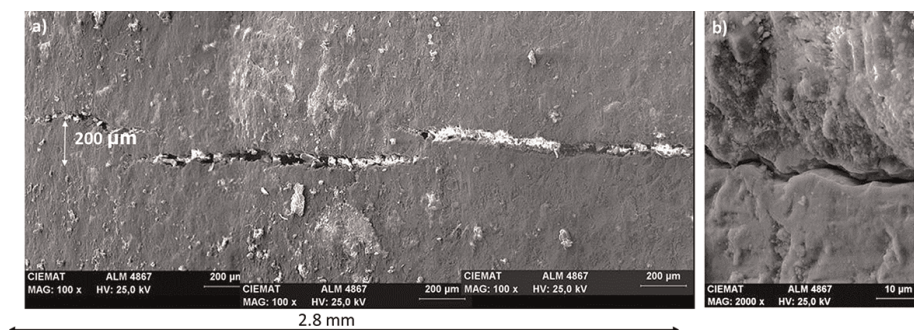


Figure 6.
 a) Circumferential cracking on OD transition zone. b) Detail of the intergranular morphology of the cracks.

3.4 Fracture Surface characterization

The tube segment with the cracks was cut into axial two halves. In one of them, a fatigue process for obtaining the fracture surfaces was performed. This fracture was examined by SEM in order to measure the length and depth of the open cracks. Two fractures were identified and these were formed by small cracking linked between them by ductile ligaments. Dimensions of both cracks are summarized in **Table 7**.

Morphology of the fracture is shown in **Figure 7**. Crack A presents an intergranular morphology with several ductile ligaments. Maximum depth of the intergranular crack was 937 µm, 82% of the tube thickness. Crack B, also of intergranular

Crack measurements	Crack A	Crack B
Length	10 mm	6.5 mm
Average depth from OD	637 µm (56%)	492 µm (43%)
Max. depth	937 (82%)	633 (55%)

Table 7.
 Dimensions of the fracture surface of the two cracks.

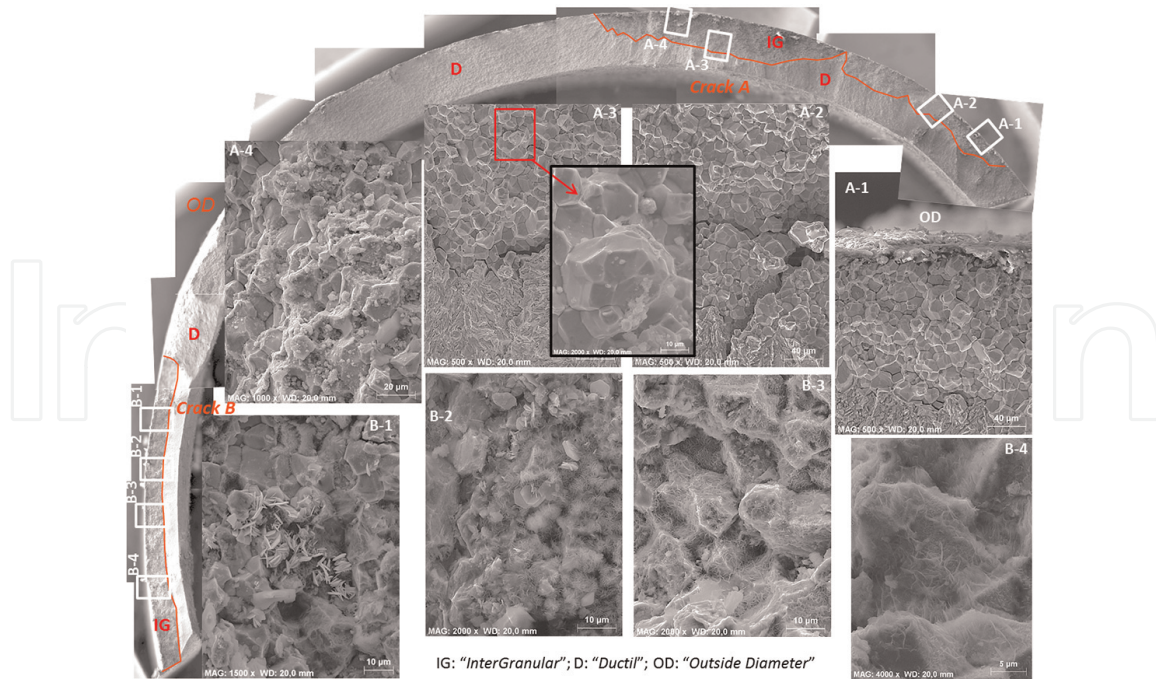


Figure 7.
 Fracture surface with details of the intergranular crack and deposits morphology (A and B).

morphology, is not complete, due to the initial cut to obtain the two halves. Maximum depth of this crack B is 55% of the tube thickness.

Intergranular morphology of the two fractures showed some different aspects between them (**Figure 7**). Fracture surface of crack B was covered by a continuous gelatinous film, while the fracture surface of crack A showed corrosion deposits only in the initial area, near the outer surface, while the remainder of the fracture was completely clean.

Significant differences in the EDX analyses of the two areas (A and B) of the fracture were not observed. Crack B has a higher sulfur average concentration than crack A. Occasional sulfur concentrations can reach 29.1% at crack B. Silicon concentrations are similar in both cracks while the chlorine concentration is higher at crack A. It should be noted that Na was not detected in any of the cracks. On the other hand, Zn is more frequently found at crack A than at crack B where only traces of this element were present. Small concentrations of barium have also been detected in the two fractures.

Metallographic characterization of selected cracks by stereoscopy microscopy was prepared in the thickness plane of the other half segment tube. **Figure 8** shows the morphology of the crack in the metallographic samples. The maximum depth detected

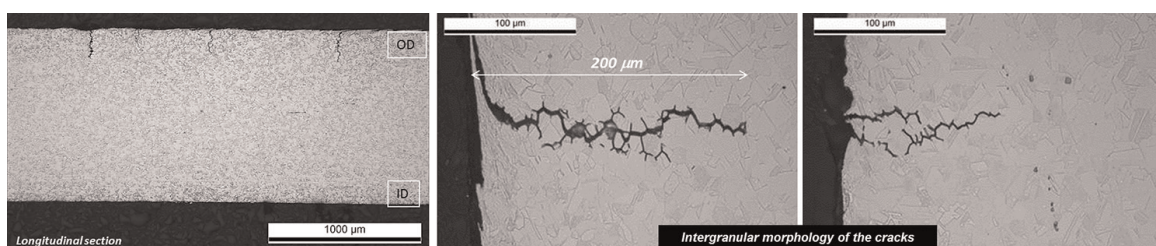


Figure 8.
 Intergranular cracks in metallographic samples.

was 210 μm , being in all cases of intergranular morphology. In one of them, it can be observed that the crack initiation is parallel to OD surface, possibly due to the existence of a hardened surface (shot peening process). In other areas, the cracks propagated with normal orientation to OD surface.

Figure 9a shows the sulfur distribution inside the cracks by x-ray mapping. In some cases, S seems to be associated with Ni or Cu and not with oxygen. It is very possible that these elements are in sulfide form. A Fe and Ni (Cr depleted) rich layer

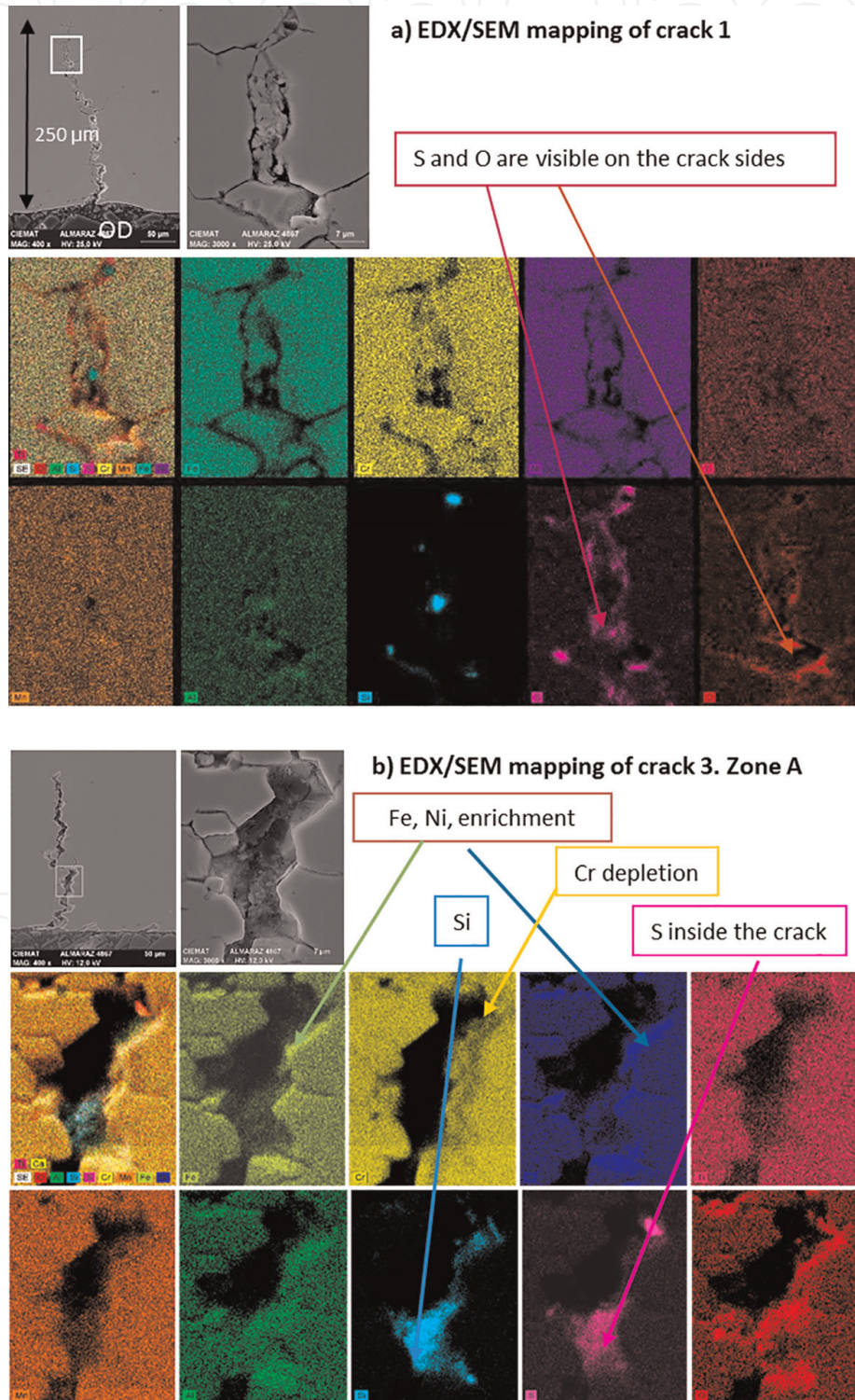


Figure 9.
a) EDX/SEM mapping of crack 1. b) EDX/SEM mapping of crack 3.

can be observed in **Figure 9b**. Besides, Si and oxygen have been detected in very internal areas of the crack. Also, the presence of S is remarkable in this area.

Deposits located on the fracture surface of cracks A and B were analyzed by Auger spectroscopy. Analyses were performed in five areas of each crack from OD to the tip of the crack. Sputtering process was performed after prior analysis in these five areas in order to observe the concentration depth profile from fracture surface to base metal. **Figure 10** shows the profiles corresponding to point 1 (near OD surface) and point 5 (bottom or tip of the crack). **Table 8** summarizes the results of these analyses where it is indicated (in nm and with arrows) the enrichment and depletion of some elements at different depths.

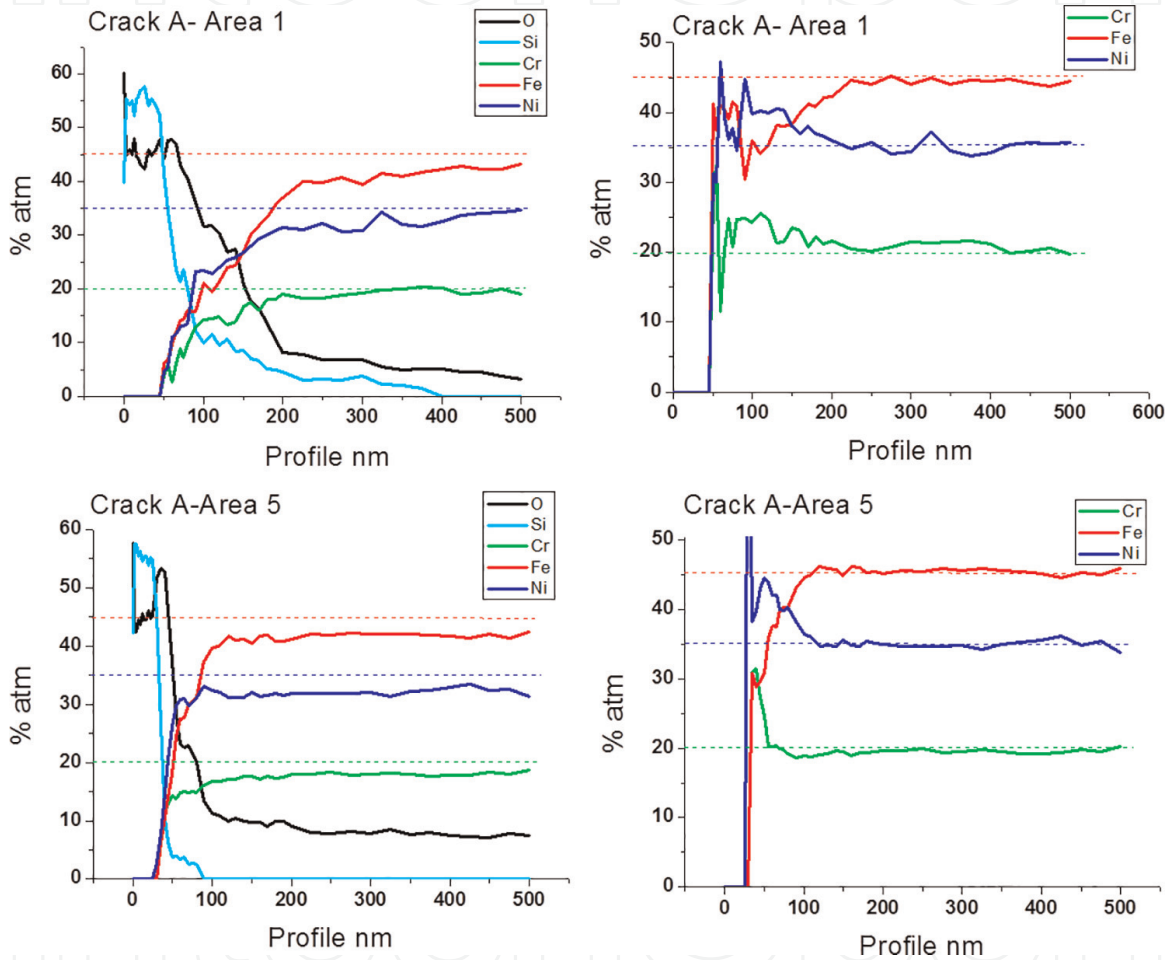


Figure 10.
 Auger profile concentration for O, Si, Cr, Fe, and Ni and Cr, Fe, and Ni. Areas 1 and 5 of crack A.

Area	Si	O	Cr	Fe	Ni
1	375	375	225 ↑	225 ↓	225 ↑
2	800	800	100 ↑ 650 ↓	250 ↓ -700 ↑	600 ↑
3	225	225	100 ↑	250 ↓	225 ↑
4	110	150	50 ↑	100 ↓	150 ↑
5	100	110	70 ↑	100 ↓	110 ↑

Table 8.
 Profile concentration summary by auger spectroscopy on the five areas of crack a. up arrow (↑) indicates enrichment and down arrow (↓) depletion, relative to base material concentration.

Concentration profiles at crack A (area 1), show a thicker silicate layer around 400 nm. This point is the closest to OD. In the other points, far from OD (area 5), the silicate layer is thinner (<100 nm). Ni enrichment is always detected at the five points of the analyses. Fe is always depleted in all cases, even though in the first layers this depletion is less pronounced. Cr is enriched in the first nm and after it is stabilized with a concentration corresponding to the base material or slightly depleted.

3.5 Sludge characterization

After sub-samples separation, M (magnetite layered), C (collars), and F (flakes) pieces were identified visually to characterize macroscopic features such as size, shape, and color. **Figure 11** shows macroscopic photographs of deposit sub-samples. Typical magnetite pieces were present as small “gravel,” generally on the order of a few millimeters in length. The colors of these pieces were grey with areas of orange tone and showed geometries and curvature compatible with the triangular shape of the space between tubes in SG tube sheet (**Figure 12**).

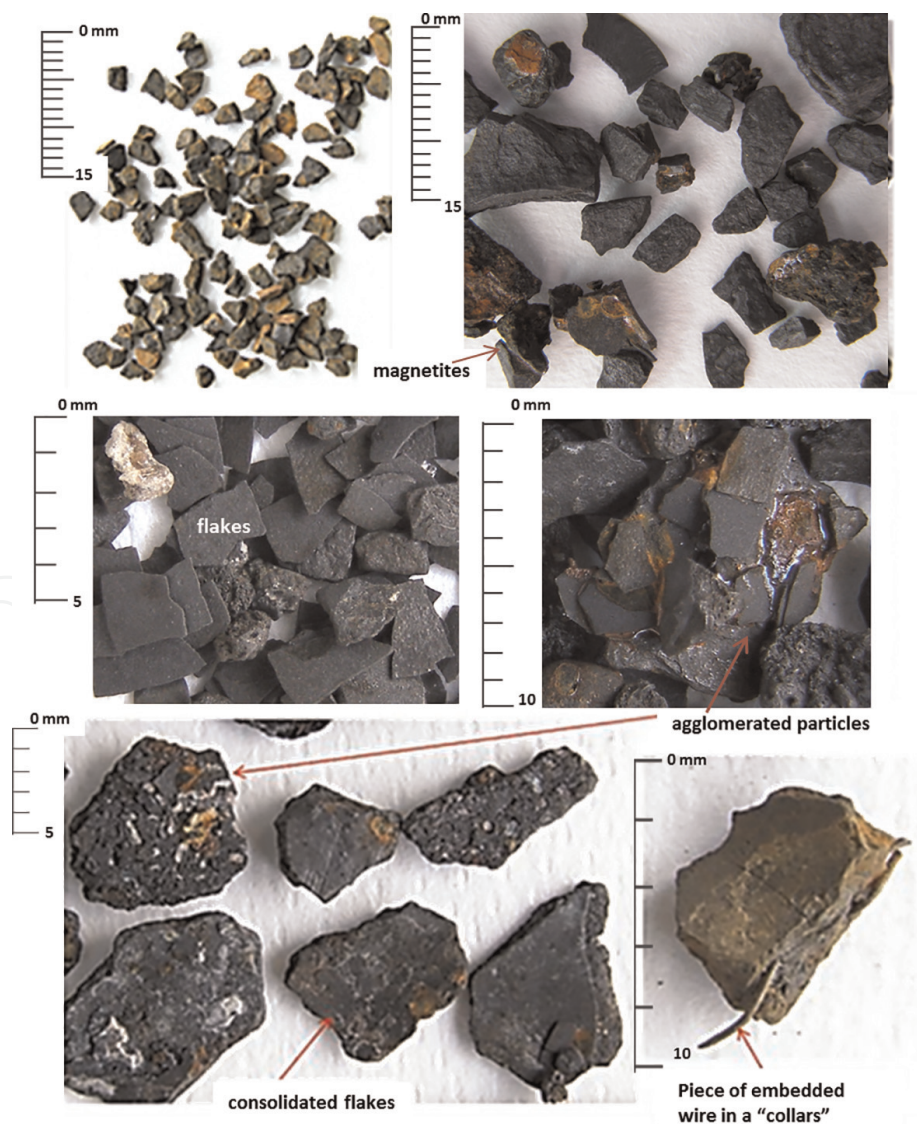


Figure 11.
Different morphology of deposits collected from steam generator.

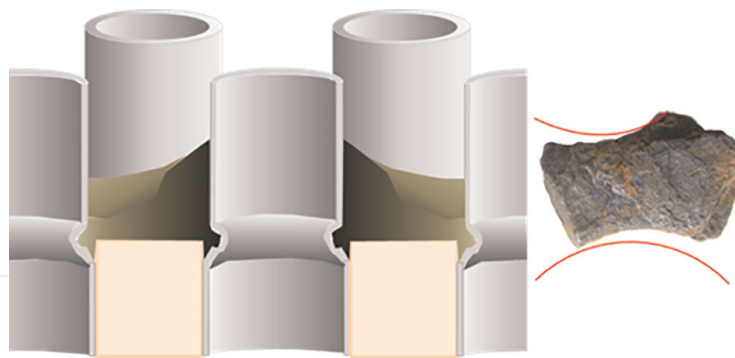


Figure 12.
Individual particle from tube-sheet SG. Dimensions fit the space between the tubes of tube sheet.

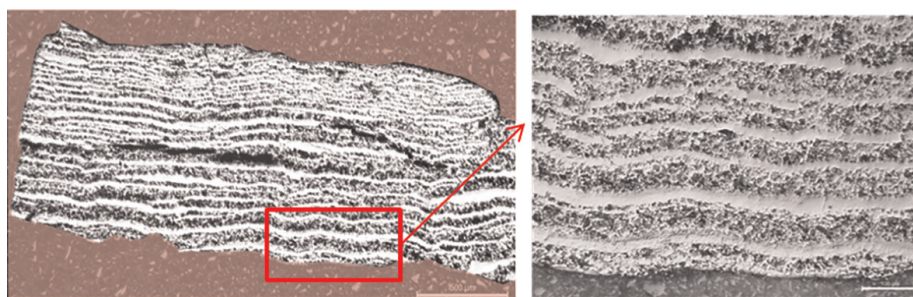


Figure 13.
Cross-section of magnetite layered particle. Optical and SEM images.

Magnetite layered pieces of several mm of thickness presented very high hardness values (876 Hv maximum). On the other hand, “flakes” present moderate hardness values (533 Hv maximum). “Collars” showed hardness slightly lower and heterogeneous values.

Most of the magnetite deposits are part of the oxide layer formed on the low carbon steel alloy and its composition is Fe_3O_4 . **Figure 13** shows the morphology in the cross-section of magnetite pieces by optical microscopy. The structure consists of alternate layers with greater or lesser porosity. In the layers with higher porosity is easy to distinguish magnetite crystals with loss of cohesion. SEM/EDX measurements were performed on the cross-section of the magnetite layered in order to quantify the concentration of the local elements at the different layers.

Figure 14 shows the elemental distribution on the magnetite layers with enriched bands in Mn. Dot analysis shows only Fe and O in the compact layers while in the porous layers exists an enrichment of Mn, Ni, Si, and other elements in a lower concentration (**Figure 15**).

The total of these elements forming the enriched bands is only 2%, the rest is Fe and O. Additional analyses performed detected an increase in S and Ni with isolated precipitates of Cu (**Figure 16**).

As discussed at the start of this section, “collars” pieces were detected Spanish NPPs (**Figure 17**). Cross-sections of these samples are formed by a number of metallic inclusions embedded in a matrix of Al and Si species (**Figure 18** and **19**). These last elements were enriched preferably near the interface with SG tube surface. Si/Al ratio is higher when the silicates are the binding agents.

Regarding “flakes” or tube scales is only observed in some NPPs before CC treatment. These particles are not detected with subsequent FFA additions and after chemical cleaning treatment.

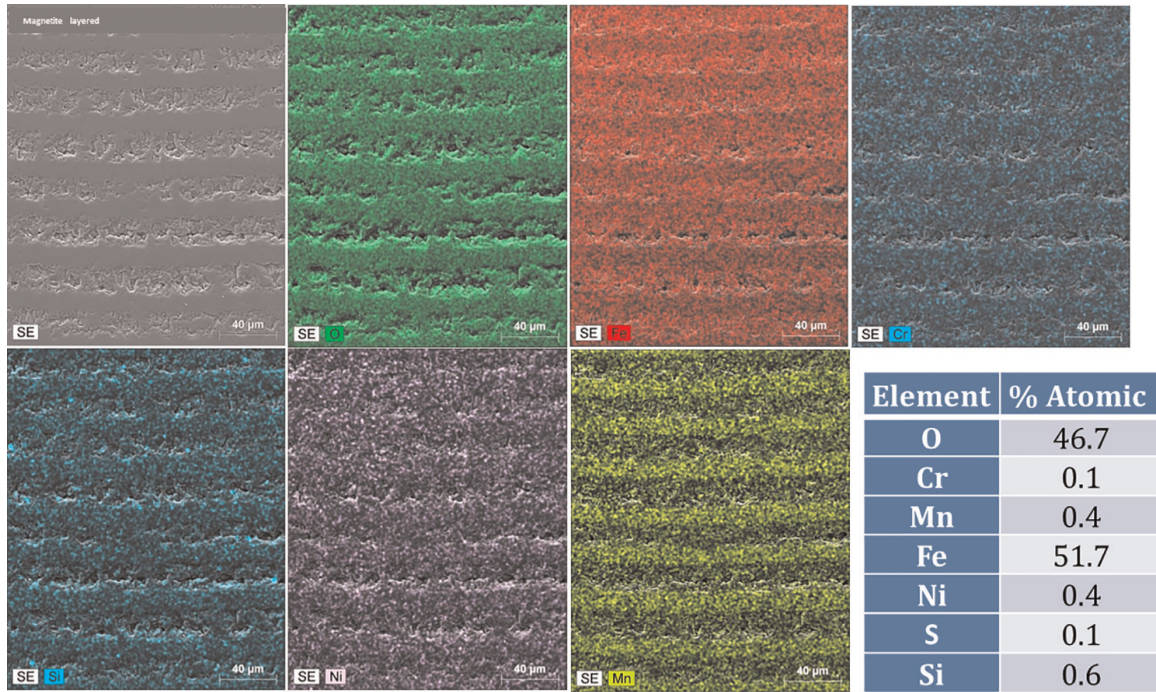


Figure 14.
Mapping of elements distribution in the cross-section of magnetite layered.

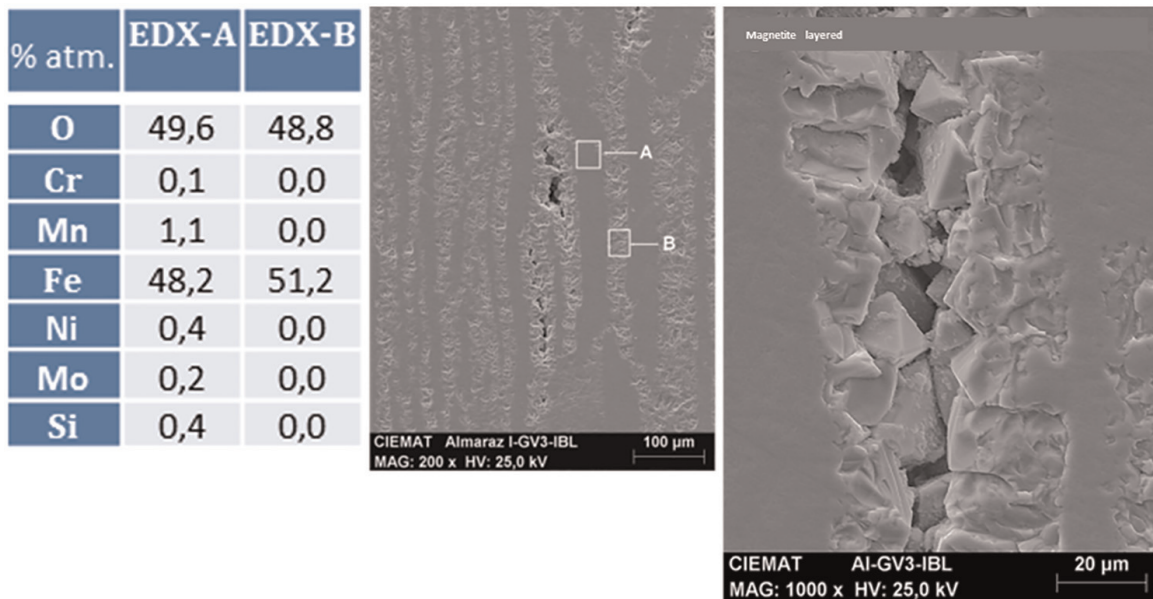


Figure 15.
Dot EDX analysis in the cross-section of magnetite layered sample.

Normally, flakes are formed by an inner layer in contact with the tubing surface and an outer layer with high porosity (**Figure 20**).

4. Failure analysis. Discussion

Alloy 800NG steam generator tubes are a composition modified austenitic stainless steel for use as steam generator tubes in PWRs. The main modifications concern the carbon content, $C < 0.03\%$ by weight, and the $Ti/C > 12$ ratios to avoid sensitization of

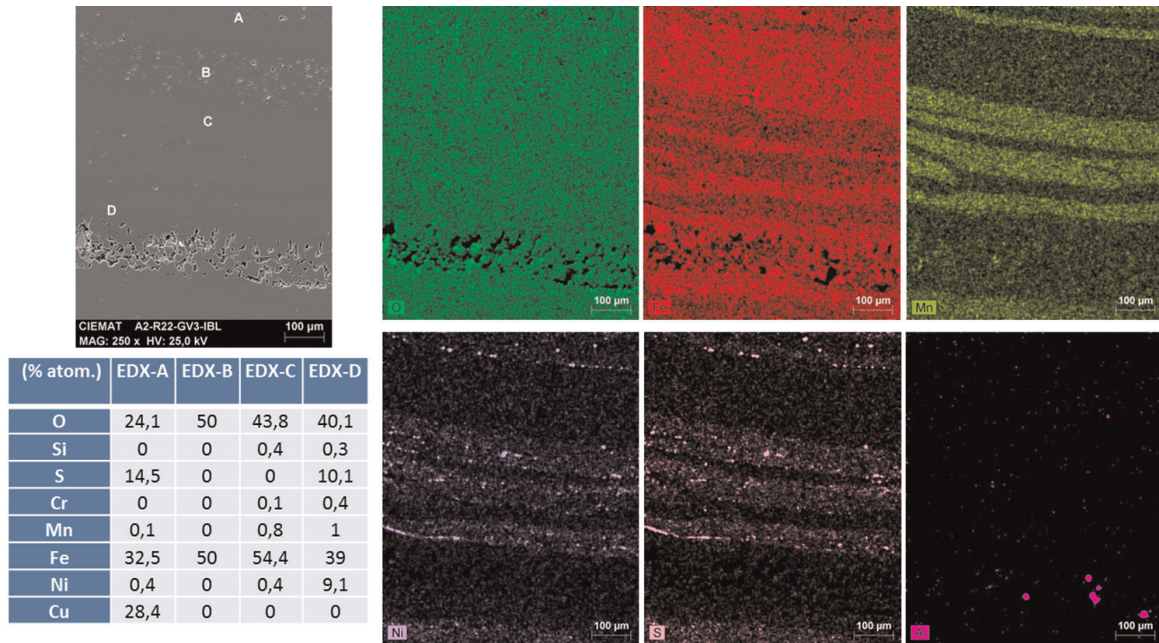


Figure 16.
 Mapping of elements distribution in the cross-section of Magnetite layered.

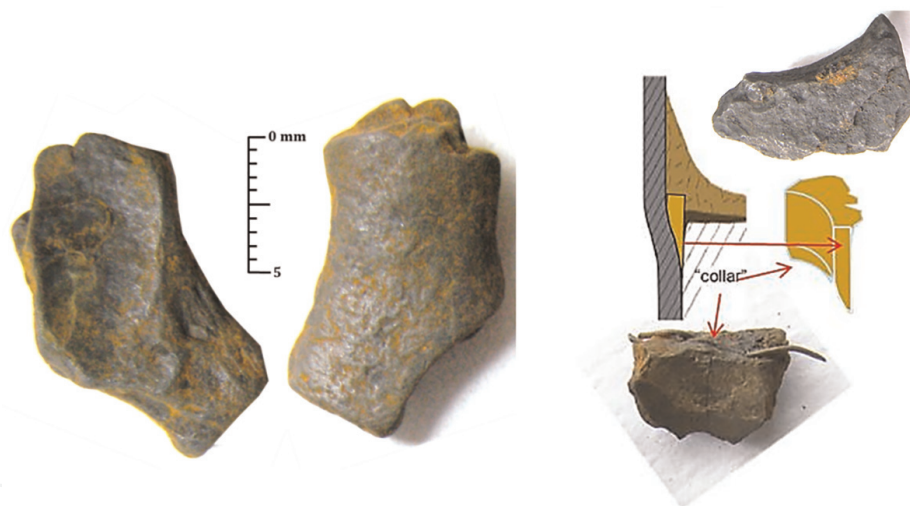


Figure 17.
 Morphology of "collars" removed from NPPs.

the material. The final stage during the tube manufacturing process is a shot-peening treatment of its external surface in order to prevent stress corrosion cracking mechanisms. The shot-peening process creates an outer layer with high plastic deformation of the surface that prevents crack propagation under SCC conditions. Circumferential cracks in the expansion transition were detected before extraction of the analyzed tube by Eddy's current inspection besides "denting" degradation and a height of sludge, about 46mm.

Destructive examination of the expansion transition zone has revealed a 5 mm wide band with multiple circumferential cracks separated by small ductile ligaments. These cracks were located 3 mm from the last point of contact between the tube and the tube sheet. No other type of damage such as "wastage," pitting or others has been detected.

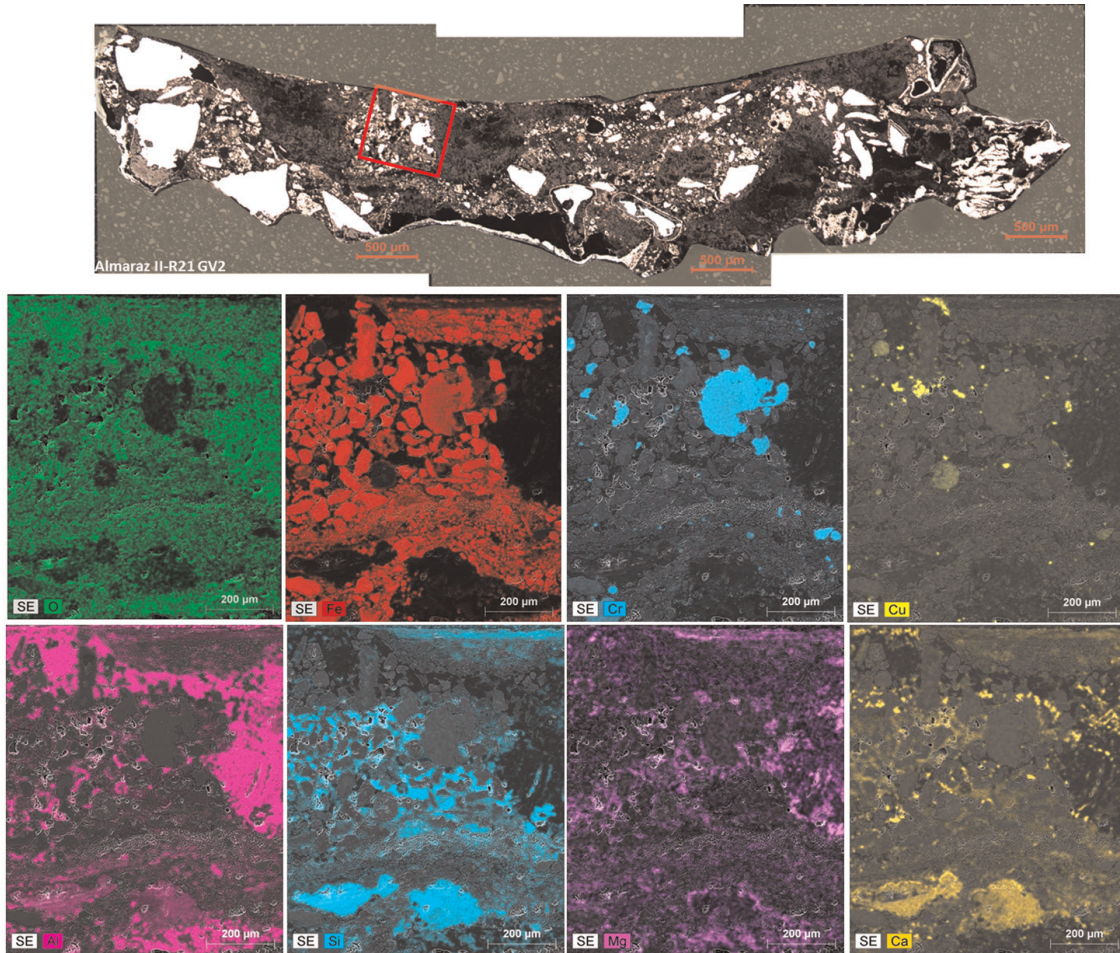


Figure 18.
Cross-section collar. Spatial distribution of chemical elements by SEM-EDX.

Two cracks have been characterized during the fractographic examination both of intergranular morphology, which at first glance presents different aspects. Crack B's fracture surface was completely covered by a viscous morphology film while crack A was covered with deposits in the initial area, near the external surface of the tube, the rest of the fracture was apparently clean.

OD-initiated corrosion of circumferential cracks in SG tubes has been described by different authors [7]. Destructive examination performed by EDF [8] found circumferential and longitudinal cracks in forty tubes examined. Circumferential cracks were located below the top of the tube sheet, while axial cracks were detected above the tube sheet under a sludge layer. The existence of “denting” was not explicitly mentioned.

Extraction of deposits from the expansion transition zone and free tube, next higher area, were compared by EDX analysis. These results indicated a process of impurities concentration in the gap between the tube sheet and the tube. Si, Mg, Ca, S, Cu, Zn, Na, and Cl were detected in this area but these concentrations were lower in the upper part of the sludge zone. It should be noted that traces of Pb have been found in some of the EDX analyses carried out on the initial area of only one of the analyzed cracks. Some authors suggest that alloy 800 could be more susceptible to SCC in alkaline solutions with lead (Pb) [9].

XPS and DRX of the extracted deposits revealed the existence of metallic Cu and FeS₂, typical water chemistry of secondary side SG. Likewise, reduced sulfur species such as sulfides or sulfites have been detected in the expansion transition zone and

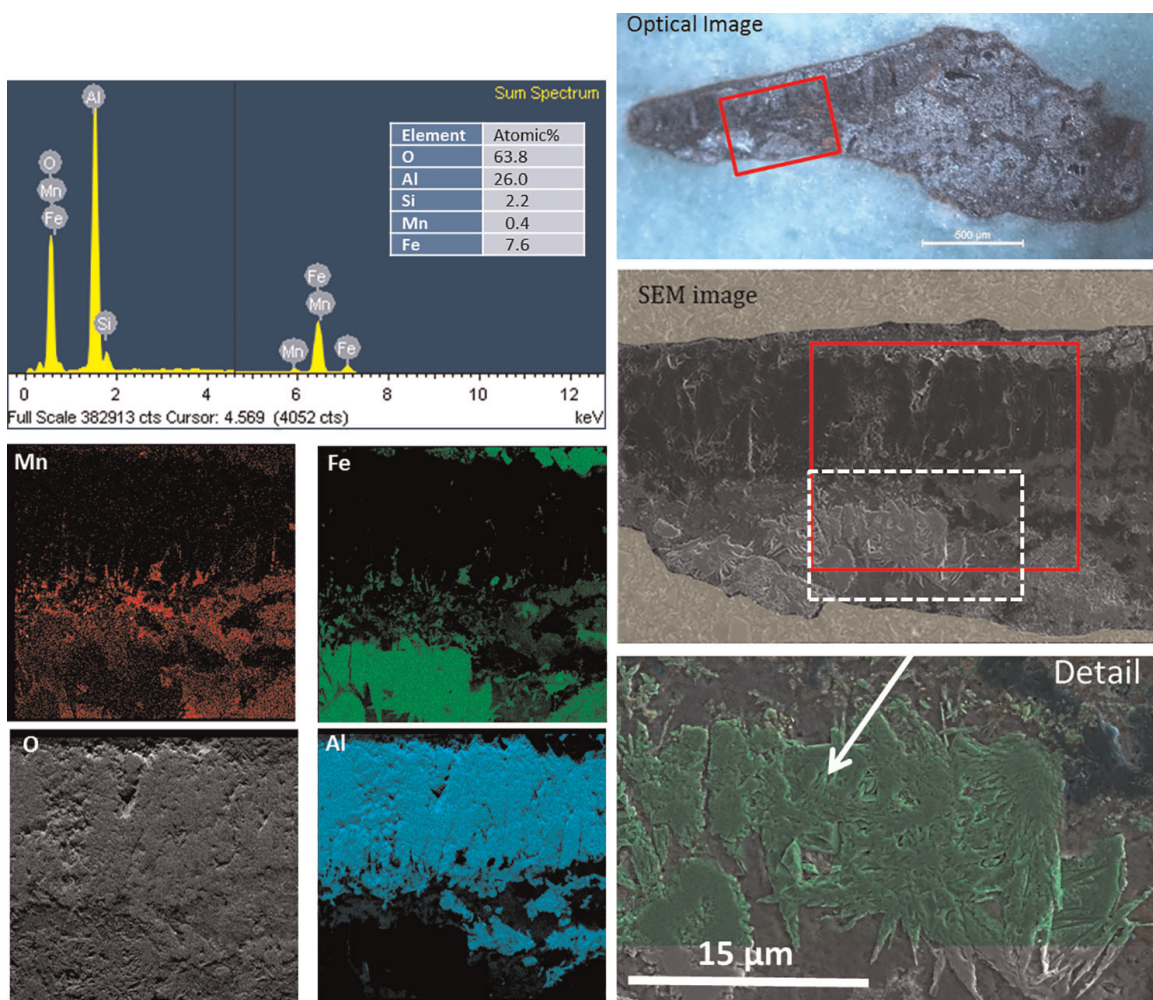


Figure 19.
 Cross-section collar. Spatial distribution of chemical elements by SEM-EDX.

under the sludge. On the other hand, XPS analyses detected the presence of Fe and Cr metallic in the free tube deposits under the sludge. In addition, there is a need to clarify the species reduction that could be produced due to ionic sputtering carried out for the analysis. However, metallic Fe has also been identified in the existing deposits in the expansion transition zone, in which ion sputtering was not carried out.

EDX analyses performed on the fracture surface of the A and B cracks confirmed the presence of impurities inside the cracks. Crack B fracture surface was completely covered by a film rich in silicates with discrete particles very rich in sulfur, besides the impurities mentioned above. However, the analyses performed in crack A revealed only deposits in the initial area of the fracture, which did not differ from those analyzed in crack B, except that they had a lower concentration of sulfur. The presence of impurities inside the cracks is also confirmed by the EDX analyses carried out inside the cracks prepared for metallographic characterization.

Silicon compounds, like silica or silicates, were continuously detected on different areas of the external surface tube and over fracture surfaces of the cracks. Many scientific papers describe the silicate's role influence in the SCC susceptibility through intergranular mechanism on the SG secondary side. Failure analyses in tubes of French plants described Al-silicate deposits over a chromium-rich brittle layer associated with corrosion damage. The presence of Al-silicates confirms that cracks formation has not been produced in strong alkaline media where this silicate is not stable

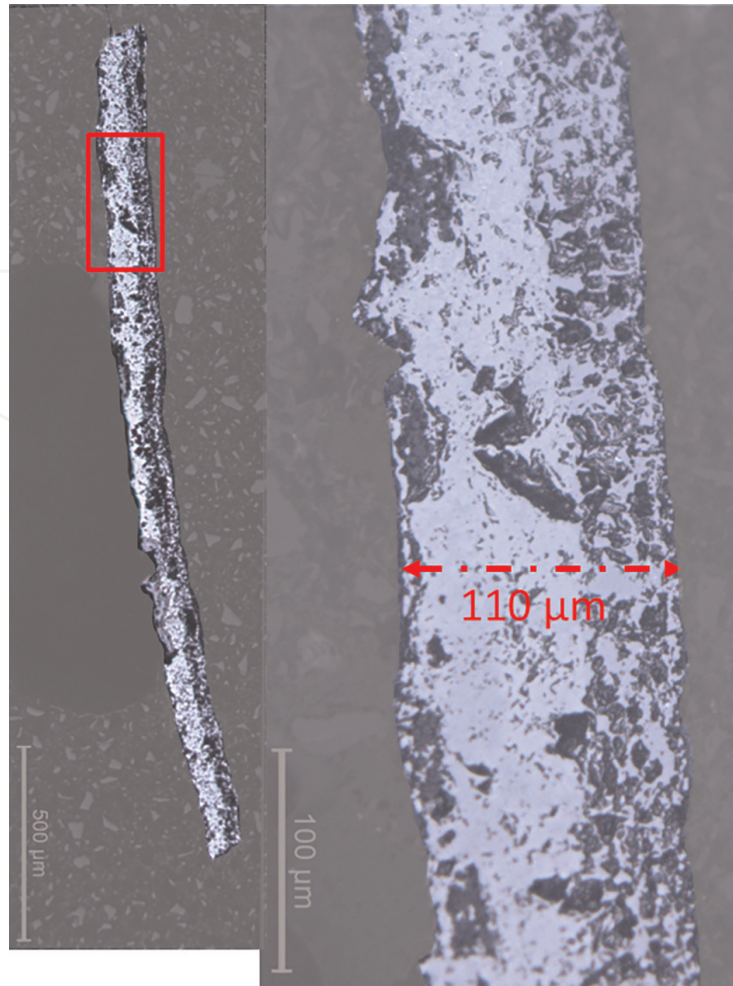


Figure 20.
Cross-section of “flake.”

(pH>10 at 300°C). EPRI (Rev.7 of the secondary guides) notes that when Si/Al ratio decreases the response of alloy 600 to IGA/SCC is worse [10]. In addition, a threshold value ~ 2 of Si/Al ratio could produce an IGA/IGSCC increase for alloy 600 MA.

In the case of alloy 800NG, deposits formation of silicates depends on microstructure. Tubes 800 NG are manufactured of Fe-base alloy. Oxide layer of this alloy expose to secondary water of PWR present a strong affinity for silica [11] and iron, even nickel can perform a cation exchange reaction with this element. Other elements such as Ca, Mg, and other alkalines can form mixed silicates producing local acid in the environments and contributing to increasing corrosion mechanisms due to the formation of protons. This mechanism could perform under the deposits in contact with an external surface of the tube due to the inhibitory capacity of silica as is demonstrated in the results of plants.

However, the silicate's role is unknown in the SCC of Incoloy 800. In fact, laboratory results show that the formation of the Al-silicate layers depends on the microstructure. These layers are very thin when they are formed on rich-chromium film, thicker on rich-nickel film, and 20–30 times thicker on rich-Fe film. Iron is the major element in Incoloy 800 it has a strong affinity for silica. In this way, iron can migrate with the Al-silicate by cation exchange reaction. Similar behavior can be attributed to nickel but this mechanism is not observed for the chromium. Meanwhile, calcium is fixed on the surface of silicates. This type of reaction can produce local acid in the environment under the deposits and contribute to material dissolution [8].

Furthermore, silica is considered an element with inhibitory capacity. This remark is based on the results of plants where lower levels of IGA/SCC were produced when silica above 40 ppb was detected during the blowdown [5].

On the other hand, many experiments have been carried out related to the effect of sulfur in different alloys for steam generator tubes in the middle of the secondary with the aim of carrying out comparative tests between alloys 600, 690, and 800. Most of the tests in the laboratory cannot be extrapolated to plant conditions, but they provide a study of the resistance of these alloys in a certain medium with sulfur species, such as sulfates in an acid medium. For example, alloy 800 was susceptible to IGSCC in a sulfate acid environment (pH = 4, at room temperature). This susceptibility was increased when the pH was lower. On the other hand, the alloy 600 produced wastage in an acid sulfate environment as was demonstrated in tests performed at CIEMAT labs in "model boiler test" [12].

The behavior of alloy 800 NG secondary water chemistry of PWR with sulfates in a neutral or slightly alkaline environment has been studied by Bouvier of EDF [13]. The dilution used was intended to be representative of existing environments in flow restricted areas and consisted of deionized water with additions of sulfuric acid and caustic soda to achieve pH between 5 and 9.5 at 320°C and sulfate concentrations of 100ppm, 5000ppm (0.05M), and 57000ppm (0.6M). Alloy 800 exhibited IGSCC / IGA in the 0.05 and 0.6 M sulfate solutions at pH=5, while no damage was observed at pH 6. Cracking was only observed in slightly polarized specimens (+100mV/Ecorr), contrary to what was observed in caustic media [14], where copper significantly increases the aggressiveness of the solution for alloy 800. Results obtained by Westinghouse also indicate that the presence of 0.6M sulfate concentrations has no accelerating effect on the stress corrosion cracking of alloy 800 at pH 6 to 8 at 320°C, while it has a significant effect at pH 5 [15]. In summary, one would only expect a significant contribution of sulfur species to the cracking detected in an acidic pH medium, which if present should have been identified by the presence of chromium-rich oxide layers in the corroded zones or some type of damage, as dissolution of material in typical of acidic media [16].

The results of the EDX analyses and Auger analyses carried out on the fracture surfaces of cracks A and B allow us to infer the medium in which the cracks have been formed. For this purpose, the concentration profiles obtained on cracks A and B with those obtained on samples tested in the laboratory were compared (**Figure 21**). In acidic media, a first layer rich in iron and nickel is observed, which is identified as a layer deposited on the specimen during cooling, and below it a layer with enrichment in chromium and depletion in nickel and iron is visible. In caustic media, an oxide

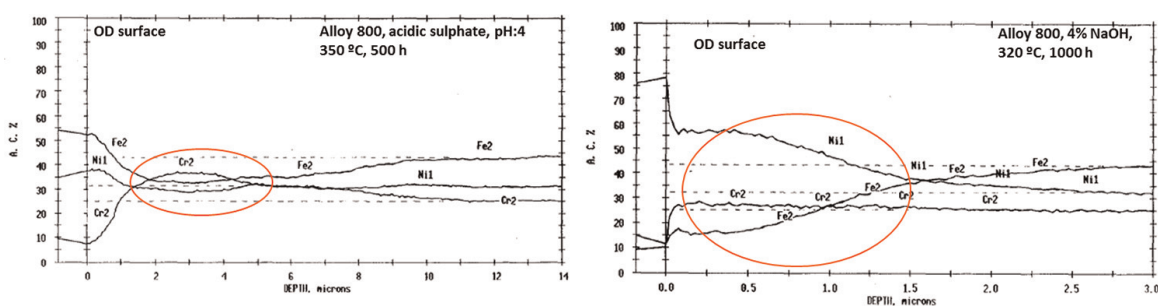


Figure 21. Auger analyses. Concentration profile of deposits formed on the external surface of a C-ring specimen tested in acid sulfates at pH =4 at room temperature and in caustic media.

layer with clear nickel enrichment, slight chromium enrichment in its outermost part, and iron impoverishment is observed.

Figure 22 shows the concentration profiles obtained on the crack fracture surface formed in an Incoloy 800 tube tested in a "model boiler" in the laboratory, in acid sulfate media, with pH=4, at room temperature.

If we compare these results with the concentration profiles obtained at the bottom of cracks A and B (**Figure 21**), we observe that the main difference between these curves and those of the laboratory sample is the existence of nickel enrichment in the latter, which, as shown in **Figure 23**, is the typical trace left by alkaline environments.

Therefore, we can conclude that the cracks have been formed in a neutral or slightly alkaline environment. Alkaline environments with pH > 10 can be discarded due to the presence of silicates. Sulfur presence would suggest acidic environments, although this evidence is not fully conclusive in all performed analyses. However,

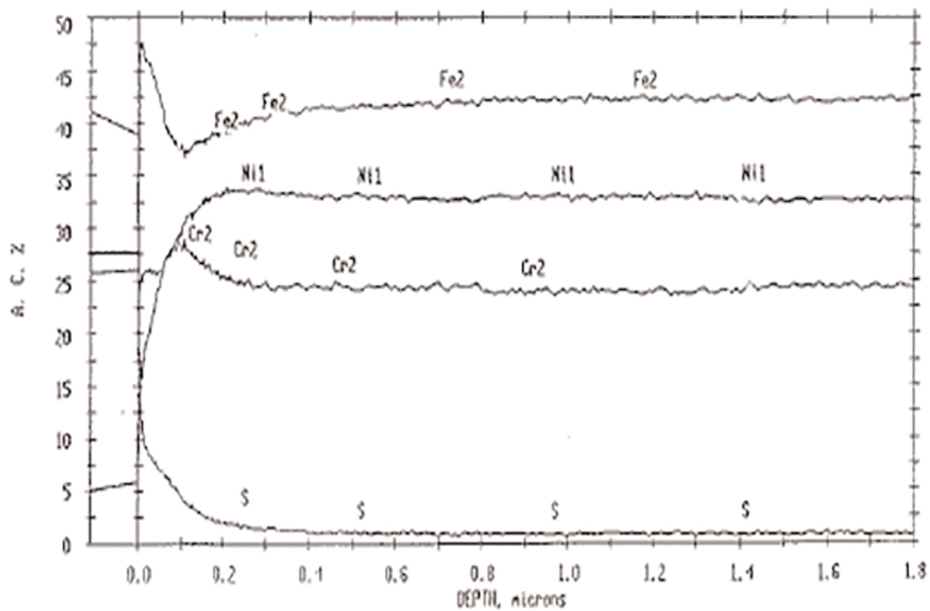


Figure 22. Auger analyses. Concentration profiles of the oxides at the bottom of a crack in an Incoloy 800 tube were tested in a model boiler in acid sulfate media.

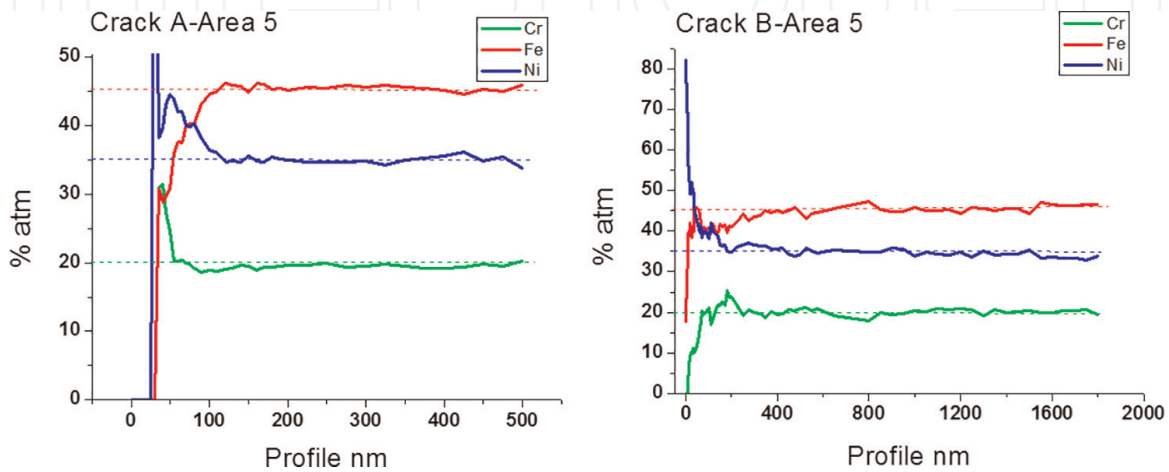


Figure 23. Concentration profiles obtained in the segment of the tube on the fracture surface of cracks A and B in the area near the bottom of the crack.

since at pH =5, sulfates considerably increase the susceptibility of alloy 800 to IGSCC, although in significant concentrations, we cannot rule out the widespread presence of sulfur in the deposits and oxide layers on the external surface and inside the cracks did not enhance the stress corrosion cracking process to some extent. In addition, it must be considered that, as a consequence of the expansion tube and shot peening process, the susceptibility to SCC in the expansion transition zone would have been higher than the tube-free zone contributing to an increase in the denting mechanism [17].

Regarding sludge characterization of particles collected on the tube-sheet as a result of secondary water chemical used, it should be noted that a root or contributing cause for the degradation mode by denting is produced by magnetite deposition over the tube-sheet surface (known as steam generator fouling). Flow accelerated corrosion (FAC) is the main source of iron from carbon steels and low alloy steels, which causes deposition in the secondary cycle. FAC is an electrolytic process where a mass transfer is produced between oxide/fluid interfaces. The most dominant variables are temperature, fluid velocity, fluid pH, the water amine, oxygen content, steam quality, void fraction of the fluid, piping geometry, and the pipe material composition [18]. Deposition process can be approached as a chemical and physical process where crystallization mechanisms and adhesion of solid particles to the surface are carried out. Soluble iron is deposited on the surfaces when the solubility of the iron decreases. It has been suggested that soluble iron can bind magnetite particles (consolidation) and reduce their re-entrainment [19, 20].

Magnetite solubility is very strongly dependent on both pH and temperature (**Figure 24**). For 300°C there is a minimum in solubility (about 5·10⁻⁹ M) found at about pH₃₀₀=7. However, the solubility increases one order of magnitude with the change of one unit of pH at 300°C in both directions [21]. As a rule, the magnetite solubility presents a minimum value for each temperature and pH, diminishing for lower temperatures and higher pH. This is why efforts to avoid the deposition of magnetite by ETA injection before shutdown and, thus, reduce the magnetite solubility and FAC. Obviously, if the amount of iron in solution is high the magnetite deposition will occur during the shutdown, especially in the cold legs. Magnetite layer is formed by a competitive process between deposition and solubility due to the small variations around this minimum of the solubility.

A protective layer of magnetite can increase during normal operation of the plants, by these previous arguments, up to a certain thickness from which magnetite layer spallation is produced. This would explain the structure found in samples named magnetite layered where alternate layers are formed during the oxidation process of low carbon steels (tube sheet). A first oxide layer is initially composed mainly of iron and oxygen and other alloying elements that depending on their different diffusion coefficients will form enriched layers in the oxide microstructure. The thickness of this first oxide layer can increase during operation up to a limit depending on several factors: temperature, environment, and time. This process will lead to a rise in the stress between a metal surface and oxide layer. When the stress in the scale increases to the limit accommodated by elastic strain, it will deform or fracture. The spallation of the scale removes its protective function allowing direct access of the environment to the metal beneath and leads to a rapid increase in oxidation forming a second oxide layer. During the oxidation, the stresses can grow due to the different specific volumes of the oxide and the volume of the metal being consumed in the reaction, which can also be influenced by specimen geometry. Moreover, thermal stresses caused by differential thermal expansion or contraction in the oxide and the substrate during temperature change can also lift the oxide layer. FFA additions can increase the

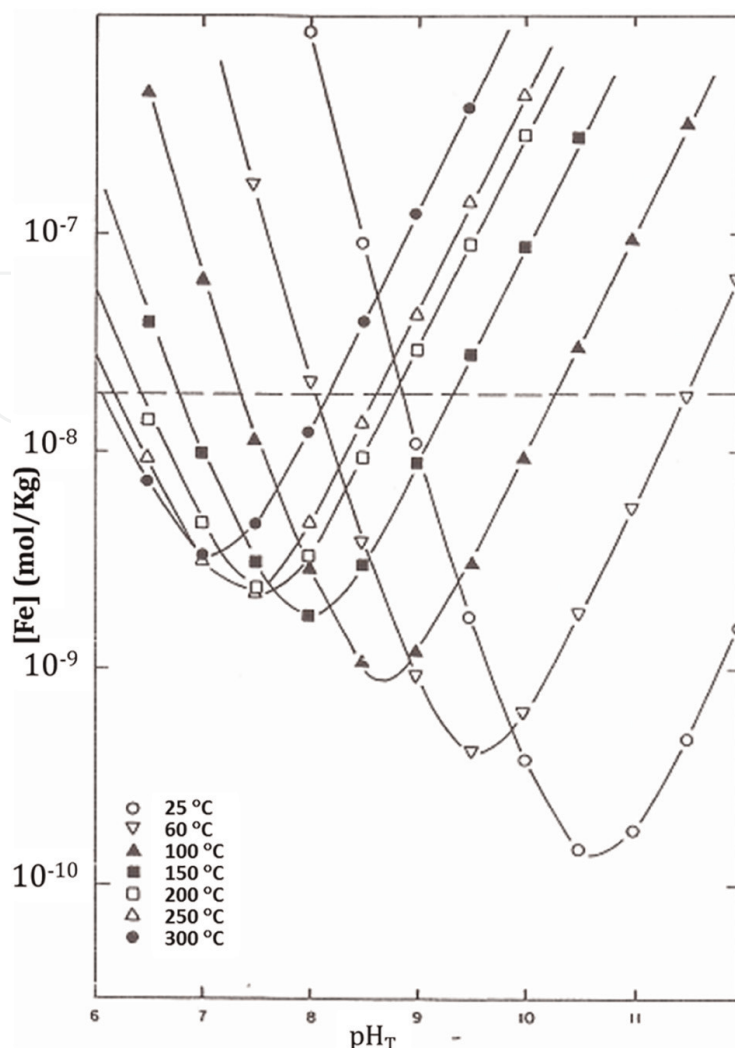


Figure 24.

Calculated solubilities of magnetite as a function of pH over the temperature range 25°C–300°C. $p\{H_2\} = 1 \text{ atm}$ [20].

spallation process due to hydrophobic behavior over the low carbon steel surface. This is one of the main reasons why the magnetite layered samples represent the highest fraction of the deposits collected.

Low Si/Al ratios have been associated with an increased risk of degradation of Alloy 600 MA tubing but no evidence for Alloy 800 tubing because this alloy is much more resistant to SCC. However, binding agents may promote the sludge consolidation, particularly in the “collars,” increasing the concentration of minor species as potential impurities for the tubing degradation [10]. On the other hand, metallic inclusions embedded in the collar matrix have been attributed to denting process when they are oxidized, although not all inclusions detected were associated with alloys with a low resistance to corrosion. Some metallic inclusions came through stainless steel or stellites. Moreover, scales formed during operation on the external tubing surface are composed of a silicate inner layer in contact with the tube surface and a magnetite outer layer with high porosity. In this way, magnetite is always present in the composition of the different types of collected samples in the sludge and its consolidation.

As is seen in the previous figures, the formation of the “collars” depends mainly on the silicon and aluminum concentration. These elements are initially in form of

colloids or aggregates of colloids and they may be oxides, oxyhydroxides, or mixed. The size of the colloids depends mainly on the environmental conditions: pH and temperature. Colloids with a large surface area produce a strong interaction with surface oxides, such as tube-sheet or SG tubing. This interaction is subjected to two main types of forces: “van der Waals” and “electrostatic repulsion” due to the presence of their surface charges. There are several theories that exist to explain the interaction between colloids and the coolant ingredients, or otherwise, the sum of the van der Waals and electrostatic interaction potentials between particle pairs. This mechanism forms the basis of the well-known Derjaguin–Landau–Verwey–Overbeek (DLVO) theory for colloid stability [22, 23]. The final result of this mechanism is a consolidation process of the deposits over the tube sheet that leads to the formation of hard sludge or “collars,” which are responsible mainly for the mechanism of denting.

Since denting needs a sludge accumulation plus contaminants and ODSCC is closely related to that, some strategies of NPP are focused on: a) Reducing the contaminants intake into SG; b) Decreasing the entry of erosion-corrosion products into SGs by means of FFA injection before shutdown and ETA injection during normal operation; c) Removing the accumulated sludge, especially hard sludge from the SG’s during outages by lancing and inner bundle lancing.

On the other hand, chemical cleaning process is used to remove magnetite from the tube scale and hard tube-sheet deposits accumulated on the tube-sheet surface. However, a high concentration of silicon and aluminum was found, due to the higher temperatures at the interface of the collar and tube or tube sheet precluded the removal of the hard sludge with chemical cleaning at the dented areas in the hot leg sludge piles. Moreover, dissolution rates vary with the surface area of the deposit available to the solvent and, therefore, tube-sheet and crevice deposits will dissolve slowly if the surface area deposits are low [24].

5. Conclusion

Failure analysis of an SG tube was performed in order to know the degradation mechanisms that occurred during the operation. Samples of sludge piles were collected during sludge lancing cleanings to understand the nature of these deposits. Several types of samples were detected: Magnetite layered, “collars” associated with Si/Al ratio, and tube scale “flakes.” Sample morphology was associated with a hard sludge, for example the “collars,” related to impurities intake into SG, like silicon, aluminum, and iron. Iron is ingressing in the secondary side of SG due to oxidant conditions and maintenance work and during refueling. Carbon steels and low alloy steels are the components with a greater contribution of iron at a secondary cycle by flow accelerated corrosion (FAC) process. Specific chemical conditions produced in the tube-sheet of SG on the secondary side lead to the precipitation of soluble species and solid particles performing denting mechanism by hard sludge, which is the prelude of SCC. Due to these facts, multiple intergranular cracks were formed in the OD located at 3 mm above the last contact point between the tube and the TS, practically in the whole perimeter of the tube. The fracture surface of these cracks was partially covered by a silicon-rich layer and sulfur. EDX and Auger analyses point out Ni enrichment with slight Cr enrichment and Fe depletion. These results are compatible with neutral or moderately caustic environments evidenced by comparative analyses performed for Alloy 800 tested in caustic and acid sulfate environments.

6. Recommendations

Measures to prevent the impurities intake into SG and performing a chemical cleaning process are actions that should be taken into account to avoid sludge formation.

Acknowledgements

The authors would like to acknowledge Spanish NNPs for providing the study materials.

Conflict of interest


The authors declare no conflict of interest.

Author details

Gonzalo Diego* and Susana Merino
CIEMAT, Madrid, Spain

*Address all correspondence to: g.diego@ciemat.es

IntechOpen

© 2022 The Author(s). Licensee IntechOpen. This chapter is distributed under the terms of the Creative Commons Attribution License (<http://creativecommons.org/licenses/by/3.0>), which permits unrestricted use, distribution, and reproduction in any medium, provided the original work is properly cited. 

References

- [1] Pugh JW, Nisbet JD. A study of the iron-chromium-nickel ternary system. *JOM*. 1950;2:268-276
- [2] Feldman H, Wolfe R. Advanced nuclear technology: Alloy 690 steam generator tubing specification sourcebook. 2016. EPRI report: 3002009412. Available from: <https://www.epri.com/research/products/000000003002009412>
- [3] Hickling J, King C. Materials Reliability Program Resistance to PWSCC of alloys 690, 52 and 152 in Pressurized Water Reactors (MRP-11). 2004. pp 2.1-2.14, EPRI report: 1009801. Available from: <https://www.epri.com/research/products/000000000001009801>
- [4] Tavassoli AA, Colombe G. Mechanical and microstructural properties of alloy 800. *Metallurgical Materials Transaction A*. 1978;9:1203
- [5] Dehmlaei R, Shamanian M, Kermanpur A. Microstructural changes and mechanical properties of Incoloy 800 after 15 years service. *Materials Characterization*. 2009;60:246-250
- [6] Riznic J. *Steam Generators for Nuclear Power Plants*. UK, Woodhead Publishing: Elsevier Ltd; 2017
- [7] Karwoski KJ. Circumferential cracking of steam generator tubes. United States: N. p., 1997. DOI: 10.2172/477675
- [8] Boursier JM, Dupin M, Gosset P, Rouillon Y. Secondary Side Corrosion of French PWR Steam Generator Tubing: Contribution of Surface Analyses to the Understanding of the Degradation Process. Ninth International Symposium on Environmental Degradation of Materials in Nuclear Power System Water Reactors. TMS. 1999. pp. 555-565
- [9] Capell B, Wolfe R, Lumsden J, Eaker R. PbSCC of alloy 800NG steam generator tubing in alkaline environments. In: *Proceeding of: 17th International Conference on Environmental Degradation of Materials in Nuclear Power Systems – Water Reactors*. Ottawa, Canada; 2015
- [10] Feldman H. Steam Generator Management Program: Steam Generator Deposits Characterization for Steam Generator Tube Degradation prediction and Management. 2008. EPRI report: 1018249. Available from: <https://www.epri.com/research/products/000000000001018249>
- [11] Sala B, Organista M, Henry K, Erre R, Gelpi A, Cattant F, et al. Laboratory Study of Corrosion of Steam Generator Tubes: Preliminary Results. United States: NACE International; 1995
- [12] Gómez-Briceño D, García MS, Hernández F. Effect of Secondary Cycle Sulphuric Acidic Injection on Steam Generator Tubes. Fontevraud 3th International Symposium. Avignon, France: French Nuclear Energy Society; 1994. p 565.
- [13] Bouvier O, Prioux B, Vaillant F, Bouchacourt M, Lemaire P. Nickel alloy stress corrosion cracking in neutral and lightly alkaline sulfate environments. In: *Proceedings of the Ninth International Symposium on Environmental Degradation Materials in NPP*. California: TMS; 1999. pp. 695-702
- [14] Castaño ML, Gomez-Briceño D, Esteban F. Steam generator replacement:

Inconel 690TT and Incoloy 800 mod as an alternative to Inconel 600. In: Proceedings of Eurocorr. Barcelona. pp. 447-457

[15] Staehle R, Properties of passive films on high nickel alloys as affected by low valence sulfur. Workshop on Effects of Lead and Sulfur on the Performance of Secondary Side Tubing of Steam generators in PWRs. Argonne National Laboratory, 1012780; 2005. p. 34

[16] Laire C, Platbrood G, Stubbe J. Characterization of the secondary side deposits of pulled steam generator tubes. In: Proceedings of Seventh International Symposium on Environmental Degradation Materials in NPP. Breckenridge, Colorado; 1995. pp. 387-397

[17] Wolfe R, Feldman H. Steam Generator Management Program: PWR Steam Generator Top-of-Tubesheet Denting. EPRI 3002002197. 2014. pp. 3-15. Available from: <https://www.epri.com/research/products/000000003002002197>

[18] NEA. Flow Accelerated Corrosion (FAC) of Carbon Steel & Low Alloy Steel Piping in Commercial Nuclear Power Plants. NEA/CSNI/R. 2014;6:2015

[19] Vepsäläinen M, Saario T. Magnetite Dissolution and Deposition in NPP Secondary Circuit. Espoo: VTT Technical Research Centre; 2010 VTT-R-09735-10. Available from: <https://www.vttresearch.com/sites/default/files/julkaisut/muut/2010/VTT-R-09735-10.pdf>

[20] Hermansson H-P. The stability of magnetite and its significance as a passivating film in the repository environment. SKI Report. 2004;07 Available from: https://inis.iaea.org/collection/NCLCollectionStore/_Public/42/022/42022527.pdf?r=1

[21] Macdonald DD, Shierman GR, Butler P. The thermodynamics of metal-water systems at elevated temperatures. In: Part 2: The Iron Water System. AECL-4137. Atomic Energy of Canada Ltd; 1972 Available from: https://inis.iaea.org/collection/NCLCollectionStore/_Public/04/065/4065211.pdf?r=1

[22] Derjaguin BV, Landau L. Theory of the stability of strongly charged lyophobic sols and of the adhesion of strongly charged particles in solution of electrolytes. Progress in Surface Science. 1993;43(1-4):30-59

[23] Verwey EJW, Overbeek J. Theory of the stability of lyophobic colloid. Journal of Physical Chemistry. 1947;52(3): 631-636

[24] Thomas RC. Utility Experience with Steam Generator Chemical Cleaning. 1994 EPRI TR-104553. Available from: <https://www.epri.com/research/products/TR-104553>